Materials Science Forum
ISSN: 1662-9752, Vol. 1186, pp 109-118
doi:10.4028/p-0wN0lJ

Submitted: 2025-12-22
Revised: 2026-02-13
Accepted: 2026-02-24
Online: 2026-04-16

Relating the Cold Rolling Pass Reduction to the Microstructural Evolution and Formability in DP800 Steel

Maximilian Hribsek[1,a*], Niklas Fehlemann[1,b], Irene Biermann[1,c], Sebastian Münstermann[1,d]

[1]Institute of Metal Forming, RWTH Aachen University

[a*]maximilian.hribsek@ibf.rwth-aachen.de, [b]niklas.fehlemann@ibf.rwth-aachen.de, [c]irene.biermann@ibf.rwth-aachen.de, [d]sebastian.muenstermann@ibf.rwth-aachen.de

Keywords: dual phase steel, non-proportional loading path, formability, process simulation.

Abstract. The influence of cold rolling pass schedules on the microstructural evolution, mechanical response and stress state of a DP800 base material was investigated. A micro-alloyed S355 steel with ferritic-pearlitic microstructure was subjected to identical total thickness reductions using different numbers of pass reductions. The mechanical behavior was characterized by uniaxial tensile tests while microstructural features were analyzed using **E**lectron **B**acks**s**catter **D**iffraction (EBSD) and light optical microscopy, with grain morphology quantified by elliptical approximations. All investigations are carried out on the deformed ferritic-pearlitic microstructure, before the final intercritical annealing to produce the final dual phase microstructure. Finite element simulations of the flat rolling process were conducted to evaluate the evolution of non-proportional stress states in terms of stress triaxiality and Lode angle parameter. The results show that varying the number of passes leads to subtle but systematic differences in strength and ductility together with pronounced grain elongation and strongly banded pearlite morphologies that challenge ellipsoidal grain representations. While the overall stress-state trajectories remain similar, increasing the number of passes results in smoother stress evolution with reduced stress peaks. These findings highlight the non-trivial role of pass scheduling in shaping deformation-induced microstructures prior to annealing.

Introduction

To understand how modern steels can be optimally processed, it is essential to quantify how each individual processing step influences the evolving microstructure and thus the resulting material properties. In dual-phase steels, even at constant chemical composition, the sequence of hot rolling, cooling, cold rolling and intercritical annealing provides numerous parameters for tailoring microstructure and mechanical behavior through controlled thermomechanical processing. Previous work by Fehlemann et al. demonstrated that the number of pass reductions during cold rolling strongly affects both the ductile damage induced during forming and the impact toughness of the final DP steel [1,2]. While those studies primarily compared different processing strategies based on the final material state at the end of the process chain after the intercritical annealing step, the present work focuses on the cold-rolled DP base material with its ferritic-pearlitic microstructure, prior to intercritical annealing. In particular, microstructural and mechanically induced differences that arise during cold rolling are investigated, while the subsequent intercritical annealing step is deliberately excluded, since it was already part of the earlier studies.

To capture those mechanical differences, which are characterized by a non-proportional loading path, it is essential to understand the underlying stress states. Local stress states are described using two scalar parameters: the stress triaxiality η and the Lode angle parameter $\bar{\theta}$, as defined in Eq. 1 and 2. The stress triaxiality is defined as the ratio of the hydrostatic stress σ_m to the equivalent von Mises stress σ_{vM} and serves as a measure of the relative contribution of volumetric to deviatoric stresses. Negative values of η correspond to compressive stress states, whereas positive values indicate tensile stress states, which are known to promote ductile damage initiation [3].

$$\eta = \frac{\sigma_m}{\sigma_{vM}} \quad (1)$$

While the stress triaxiality provides information on the tendency for damage initiation, the Lode angle parameter supplies complementary information on the shape of the stress state. It is related to the third invariant of the deviatoric stress tensor ξ [4].

$$\bar{\theta} = 1 - \frac{2}{\pi}\arccos\xi \quad (2)$$

In this work, both experimental and numerical approaches are employed to figure out the mechanisms responsible for the differences in damage evolution observed at the end of the processing chain. Uniaxial tensile tests are used to characterize the global formability of the material, microstructural features are quantified using pairplots derived from EBSD and light optical microscopy data. Finally, finite element simulations are performed to evaluate the stress states experienced by the sheet during the rolling process.

Materials & Methods

The methodology presented in the following section follows the procedure previously described by Fehlemann et al. [1]. The material investigated in this study serves as the base material for the production of a DP800 steel. Chemically, it corresponds to a micro-alloyed S355 steel, with its composition summarized in Table 1. The material was initially hot rolled on a universal two-high rolling mill (Buehler). Starting from an initial thickness of 140 mm, it was reduced to 3 mm over 18 passes. The rolling process begun once the material reached a temperature of 1200 °C. After hot rolling, the sheet was cooled inside the furnace for 24 hours to ensure the formation of a ferritic-pearlitic microstructure. To achieve the surface quality required for subsequent cold rolling, the sheets were than sandblasted. Cold rolling was performed on a four-high mill to a final thickness of 1.5 mm, using three different pass schedules. The first schedule involved an initial reduction of $\Delta h_{1,1}$ = 1 mm, followed by a second reduction of $\Delta h_{1,2}$ = 0.5 mm, resulting in a total of two passes. The non-uniform two-pass rolling schedule was intentionally selected to maximize the reduction per pass while minimizing the number of passes. High single-pass reductions are known to promote pronounced through-thickness gradients in residual stress and microstructure, whereas multiple small reductions tend to deform more homogeneity [5]. Thus, the remaining two schedules applied constant pass reductions of Δh_2 = 0.3 mm and Δh_3 = 0.15 mm, corresponding to five and ten passes, respectively. From the final cold-rolled sheet, tensile specimens were prepared as well as additional metallographic samples for the microstructural characterization.

Table 1. Chemical composition of the initial S355 steel.

Element	C	Si	Mn	Cu	Al	Mo	Ni	Cr	V	Nb	Ti	Co
Wt.%	0.1	0.4	1.8	0.05	0.03	0.02	0.05	0.2	≤0.005	0.04	0.02	0.005

Tensile tests were carried out on a ZwickRoell Z100 universal testing machine to determine the materials flow curves at a constant strain rate of 0.001 s^{-1}. For the **I**nverse **P**ole **F**igure (IPF) maps, EBSD measurements were performed on metallographic samples that had been ground, polished and subsequently electropolished using a QUETCH 1000 electrolytic polishing and etching machine using the producers K1 electrolyte to erode the surface. The measurements were taken with an accelerating Voltage of 20 kV and a current of 0.14 nA, while mapping a field of 300 × 225 µm² and a step size of 0.5 µm. The examined surfaces correspond to the RD (rolling direction) × ND (normal direction) plane. EBSD measurements were conducted using a focused ion beam scanning electron microscope, Helios 5 Hydra UX, manufactured by Thermo Fisher Scientific, equipped with an EDAX detector. Post-processing was carried out using the EDAX OIM Analysis 8™ software, where only ferrite was evaluated by filtering out all phases that do not exhibit a body-centered cubic crystal structure. Minor losses of bcc ferrite located between cementite lamellae were accepted, as they are not relevant for the subsequent microstructural evaluation. To identify and quantify the pearlite phase,

light optical microscopy was employed. Samples were polished and etched with 2 % Nital, which renders ferrite bright and pearlite dark. For each specimen, images of the RD × ND plane were recorded at a magnification of x750 using a digital VHX-1000D light microscope (Keyence Corporation), ensuring a statistically sufficient number of grains. Image processing was conducted using the OpenCV Python library in accordance to Jin et al. [6]. Following noise reduction, pearlite islands and bands were detected through contour recognition, and their shapes were approximated using elliptical fitting. In cases where pearlite bands extended across the entire image, a watershed algorithm was applied to segment the bands into individual regions. The resulting processed images enabled a reliable determination of the ferrite and pearlite phase fractions.

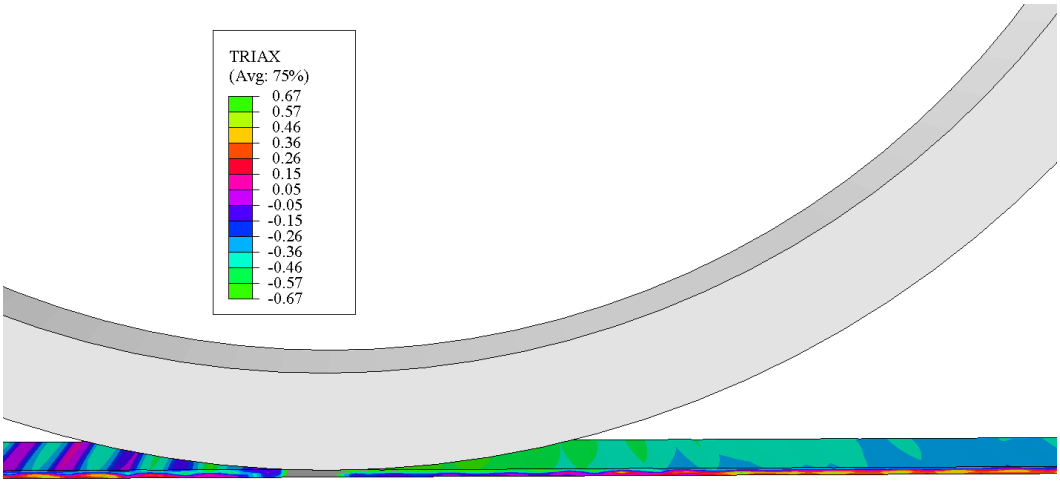

Fig. 1. Schematic illustration of the finite element model used for flat rolling.

In addition to the experimental processing, three-dimensional finite element (FE) simulations were conducted using Abaqus/Standard 2022 to analyze the stress conditions that arise during flat rolling, in a similar fashion as in Mahmoudi et al. and Wang et al. [7,8]. Figure 1 illustrates a representative stress distribution obtained from the simulations. Stress triaxiality and Lode angle parameter were evaluated after each deformation increment to characterize the local stress state throughout the process. Thermal effects were not considered, as the temperatures reached during cold rolling remain far below levels at which microstructural evolution or significant changes in the flow behavior would occur [9]. To initiate contact between the workpiece and the rollers, a rigid pusher was introduced, allowing the sheet to remain stationary without prescribing a velocity [7]. Contact interactions were modelled using a tangential penalty formulation with a friction coefficient of 0.3, while normal contact was enforced through a “hard” contact overclosure rule. For the five- and ten-pass configurations [10, 11], the C3D8R element type was selected, which is a hexagonal 8-node linear brick with reduced integration [7, 12]. This element type was chosen due to its efficiency, as it requires the least computational time. However, for the two-pass configuration, this element type was not suitable because the height reduction per pass was too large, causing excessive mesh distortion. To address this issue, the C3D10 element type was used instead [13]. This is a tetragonal 10-node quadratic element that allows for the application of remeshing rules, effectively resolving the distortion problem. For computational efficiency, the model was represented as a quarter-symmetry configuration by mirroring the geometry along the normal and transverse directions, while retaining realistic initial dimensions. [14] The simulations were carried out in a sequential manner, with each step representing a single rolling pass. After each pass, the resulting geometry was imported into the subsequent analysis, and the corresponding stress field was applied as a predefined field. This stepwise modelling strategy improved numerical stability and facilitated error detection between passes [15]. Moreover, it enabled accurate representation of the alternating rolling direction inherent to the laboratory rolling setup, which differs from industrial mills with fixed alignment.

Results

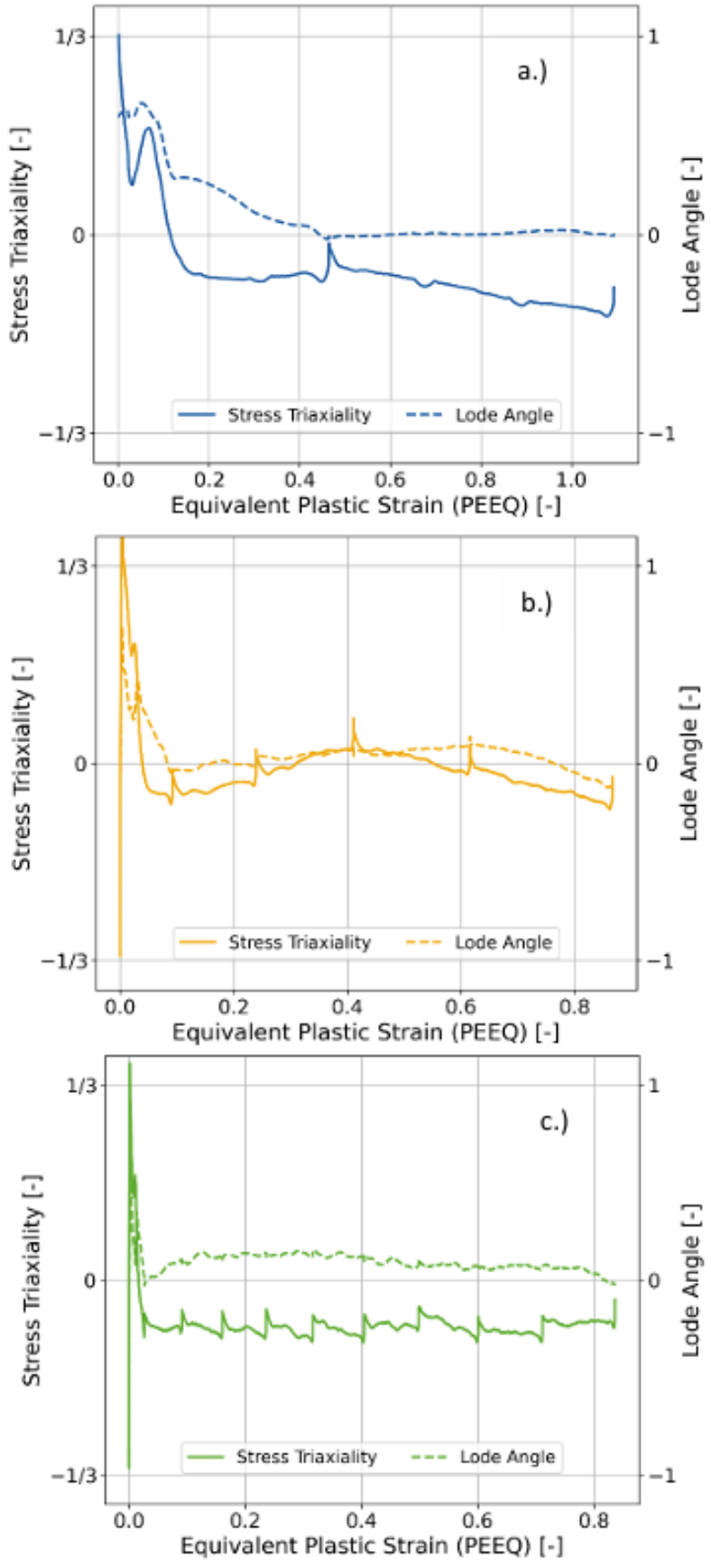

Fig. 2. Evolution of stress triaxiality and Lode parameter over the equivalent plastic strain for a.) two passes, b.) five passes and c.) ten passes.

Stress state analysis.

To capture the load paths experienced by the material during cold flat rolling, the elemental values of the entire finite element mesh were extracted and averaged over the sheet thickness and width. Figure 2 illustrates the resulting evolution of the non-proportional stress state as a function of the equivalent plastic strain for different numbers of passes. The solid line represents the evolution of the stress triaxiality, while the dashed line shows the corresponding Lode angle parameter. Three characteristic stress states are particularly noteworthy, all of which are located within the plane-stress region of the stress triaxiality - Lode angle parameter space. At a stress triaxiality of 1/3 and a Lode angle parameter of 1, the material is in uniaxial tension. When both the stress triaxiality and Lode angle parameter reach zero, the stress state corresponds to pure torsion. At a stress triaxiality of -1/3 and a Lode angle parameter of -1, the material is in uniaxial compression. For more detailed explanations of stress-state definitions and their implications, see [3].
The stress-state evolution exhibits similar gradients across all rolling conditions. In all cases, the stress response begins with an instantaneous rise into the uniaxial tension regime. This initial peak may stem from the biting conditions as the material enters the roll gap. However, it is unclear whether this behaviour reflects a numerical artefact related to the contact formulation or an actual physical phenomenon. Therefore, this peak should be interpreted with caution, and the subsequent analysis focuses primarily on the stress evolution following the first pass. Each pass can be identified by a brief increase in stress triaxiality at its onset, followed by another peak at its completion. With an increasing number of passes, the peaks in stress triaxiality become less pronounced, resulting in a smoother overall stress evolution. After the initial peak, the triaxiality transitions into the compressive regime, slightly below zero, while the Lode angle parameter remains just above zero. Only in the five-pass configuration the triaxiality briefly returns to positive values after the third pass, reaching a maximum of 0.075. The lowest triaxiality is observed in the two-pass case, reaching -0.141 at the end of the second pass, immediately before peaking again. Variations in the Lode angle parameter are similarly miner, without providing additional insight. A notable point is the accumulated plastic strain: five and ten passes yield comparable values of 0.866 and 0.836, respectively, whereas the two-pass simulation reaches 1.09. The minor difference between five and ten passes suggests a potential trend, but, considering that the overall degree of deformation is identical in all three cases, this appears unlikely.

Tensile Properties.

Tensile tests were performed to characterize the mechanical properties of the material. Because the influence of cold rolling was the primary focus, Figure 3 distinguishes between the hot-rolled and furnace cooled condition (left side), representing the state prior to cold rolling, and the cold rolled conditions with various numbers of pass reductions (right side). As no thermal treatments were applied between hot rolling and subsequent cold rolling, all observed differences in the stress-strain curves must have been induced due to mechanical deformation during rolling. The microstructure remains ferritic-pearlitic in all conditions. Consequently, variations in the curves for the cold rolled samples reflect differences in work hardening behaviour associated with the respective pass reductions. These work hardening effects explain not only the differences between the various cold rolled conditions but also their deviation from the hot rolled reference. The hot rolled material exhibits minimal scatter in yield and ultimate tensile strength, whereas the fracture strain shows considerable variability, indicating greater sensitivity of the ductility to local microstructural or geometric heterogeneities in the undeformed state When evaluated on a relative basis, a comparable scatter is also observed for the cold-rolled conditions. The yield strength reaches its maximum after two passes at approximately 825 MPa, whereas after ten passes it is about 30 MPa lower. Additionally, the fracture strain decreases by roughly 25 % when the number of passes increases from two to ten. Although these differences appear relatively small, they nonetheless suggest a trend that may indicate subtle microstructural modifications associated with varying the number of rolling passes.

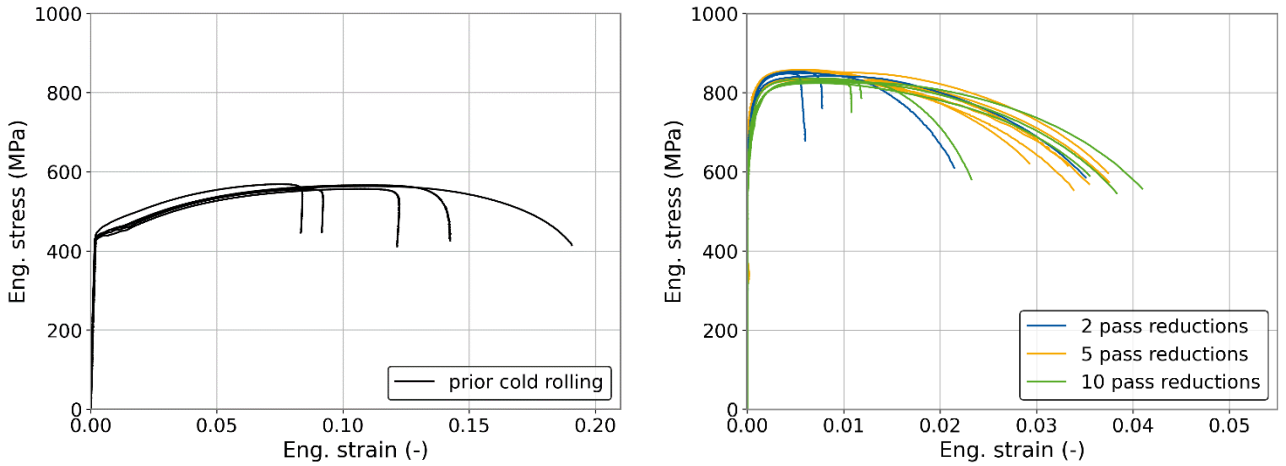

Fig. 3. Uniaxial tensile tests before (left) and after (right) cold rolling with different passes.

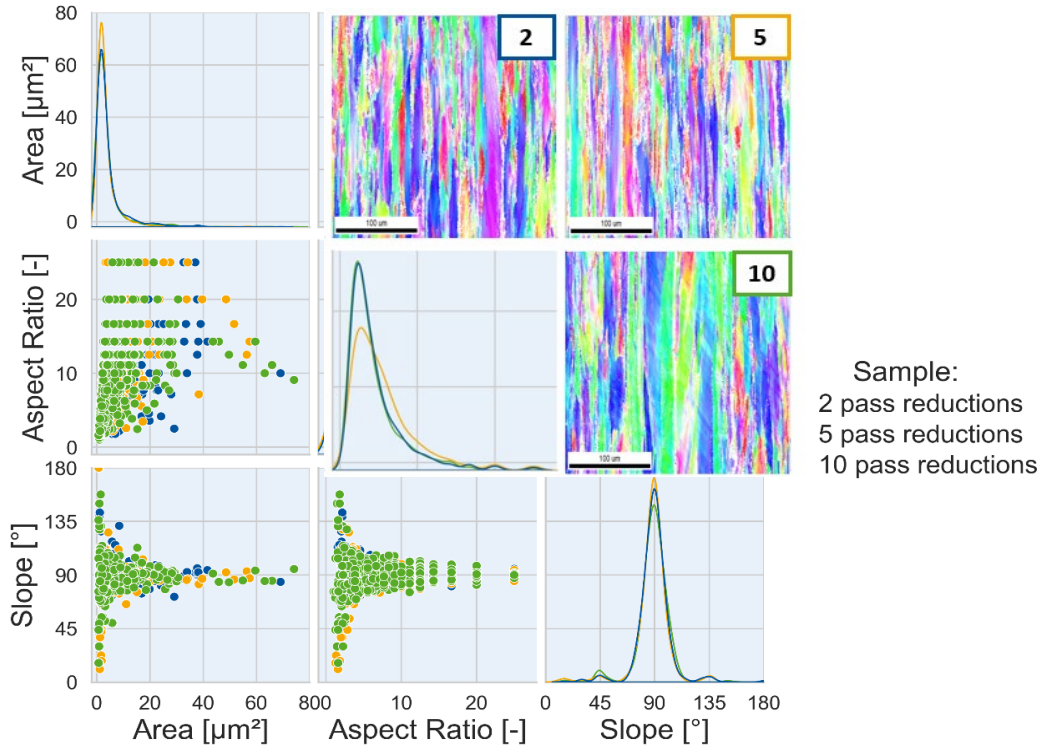

Fig. 4. Pairplot of the ferrite phase with corresponding EBSD-IPF.

Characterizing the microstructure.

To analyse the microstructural features, the samples are examined using EBSD maps and light optical microscopy. For quantification, the grains are approximated as ellipses. This approach provides a simplified geometric representation of grain shape and allows for direct comparison of different microstructures using pairplots, as shown in Figure 4 for ferrite and Figure 5 for pearlite. From there, qualitative parameters were chosen for this characterization, which are the grain area, the aspect ratio, defined as the ratio of the major to minor axis of the ellipse, and the grain slope, which describes the angle between the major axis and the x-axis of the corresponding image.

These pairplots can be divided into three regions: the upper-right corner, the diagonal, and the lower-left corner. In the uppe r-right corner, images of the individual pole figures (for ferrite) and etched surface images (for pearlite) are included to indicate the origin of the displayed information. Along the diagonal, **k**ernel **d**ensity **e**stimates (KDEs) illustrate the distributions of the three grain descriptors, while the lower-left panels show the relationships between these variables. From the KDEs, it can be seen that both the grain area and the aspect ratio follow a lognormal-type distribution across all three material configurations. The distributions are very similar, with mean grain areas

ranging from 2.67 to 2.95 µm² for two and ten passes, respectively. The mean aspect ratios lie between 4.47 and 5.66, reflecting a pronounced elongation of the ferrite grains. The grain slope consistently approaches 90°, corresponding to the rolling direction. This trend indicates that as grains align more closely with the rolling direction, their aspect ratios increase, resulting in a greater elongation along that direction.

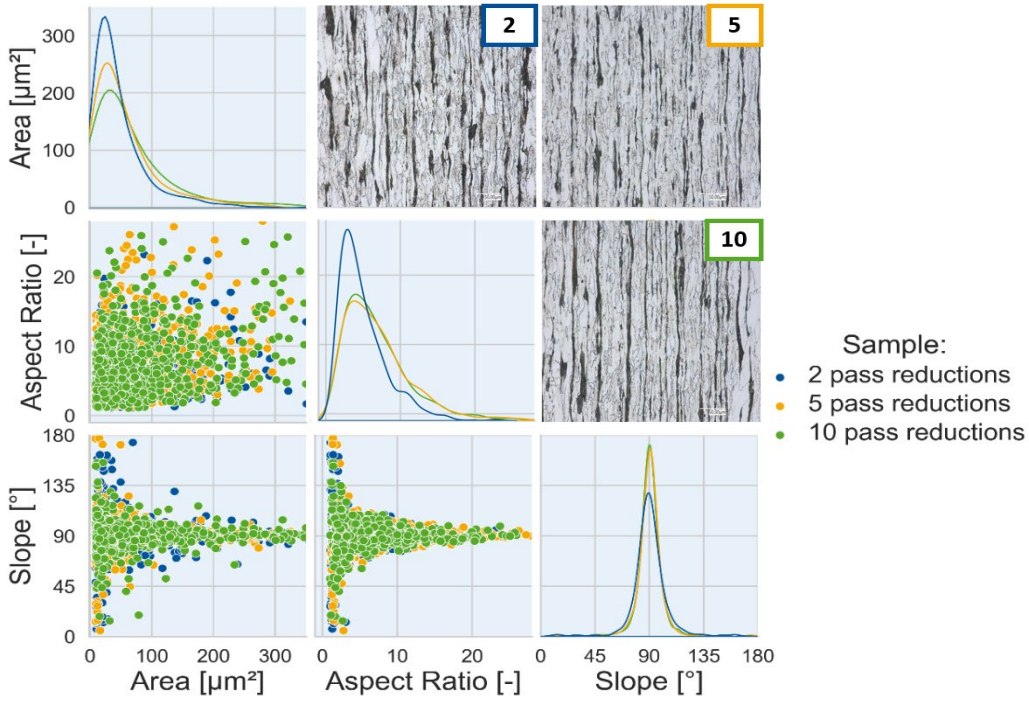

Fig. 5. Pairplot of the perlite phase with corresponding light optical images.

Comparable trends are observed for the pearlite phase, as shown in Figure 5. The grain areas are considerably larger than those in ferrite, with mean values ranging from 48.77 µm² for two passes, 66.16 µm² for five passes, up to 75.23 µm² for ten passes. This is likely due to pearlite's tendency to form banded structures, which are not easily represented by simple ellipses. Supporting this interpretation, the aspect ratios also increase, reflecting the elongated morphology of these bands.

The final microstructural feature to consider is the volume fraction of the two phases. Despite minor variations in the measured values, the pearlite fraction can be regarded as constant across all three samples due to the absence of thermal treatments. The pearlite volume fraction was determined by binarizing the light optical microscopy images, yielding values between 11.5 % and 13 %. These results are in good agreement with the pearlite content reported in the literature.

Discussion

The results demonstrate that varying the number of pass reductions alone leads to non-trivial differences in the resulting materials properties. Moreover, an evaluation of the new methods used to capture the process-structure relationship highlights promising possibilities for future investigations. While the tensile tests already indicate subtle variations in the mechanical properties, the subsequent analyses were intended to confirm these differences and to provide insight into their underlying origins. With regard to future work, the microstructural observations are particularly relevant in the context of constructing **r**epresentative **v**olume **e**lements (RVEs) for the evaluation of damage accumulation during the cold rolling process. In contrast to previous studies, such as in Fehlemann et al. [1], the present work focuses on the deformation-induced microstructure prior to intercritical annealing, where cold rolling already leads to markedly increased grain aspect ratios. As this state has not yet undergone recrystallization driven relaxation and phase transformation, the resulting microstructure is considerably more elongated than in post-annealed conditions, to a point where the perlite grains often exceed the images boundaries. This observation suggests that grains should no

longer be represented solely as idealized ellipsoids. Instead, banded microstructural features should be explicitly considered, as they are expected to play a crucial role in accurately capturing the materials response and damage evolution [16, 17]. In addition, statistical characterization approaches such as n-point correlation functions offer a promising alternative for capturing complex spatial correlations and anisotropic microstructural features beyond idealized grain geometries [18]. As discussed above, this work also employed new methods to address limitations encountered in previous studies. One such issue concerned the accuracy of EBSD imaging when polishing with a conventional OPS-polisher, as earlier investigations reported measurement uncertainties when distinguishing between different phases. To mitigate this, an electro-polishing technique was applied to improve phase contrast and overall image quality. While this approach significantly enhanced image clarity, it also led to excessive surface erosion, resulting in increased surface roughness and the appearance of blanks and bulges in the images. Consequently, this effect may have influenced the grain size evaluation and it can therefore be assumed to contribute to the comparatively small measured ferrite grain areas relative to pearlite, even though ferrite does not exhibit a banded morphology. This fact also hindered the construction of RVEs, which will be addressed in future studies.

A key aspect of this study was the investigation of the stress states occurring during the rolling process and their influence on both damage accumulation and microstructural evolution. Previous studies have shown that an increasing number of rolling passes leads to an enhanced damage tolerance in dual-phase steels, while simultaneously affecting the development of deformation induced microstructural features such as grain elongation, phase banding, and strain partitioning. Based on these findings, it can be assumed, although this still needs to be confirmed by future investigations, that the amount of accumulated damage and the resulting microstructural state already differ during the cold rolling process when different pass schedules are applied. An evaluation of the stress state analysis suggests that this behavior may be related to the evolution of stress peaks during rolling. With an increasing number of passes, the stress peaks at entry and exit of each rolling pass become less pronounced, while the overall stress progression becomes more stable. This stabilization may result in reduced stress fluctuations within the material, thereby lowering the likelihood of damage initiation during the rolling process. When comparing the obtained stress states with those reported by Wang et al. for caliber rolling [7], it can be observed that the loading conditions remain comparatively constant over the duration of deformation. This indicates that, for further analyses, it may be sufficient to investigate different areas of the sheet, for example by comparing the stress responses at the surface and in the core. Such an approach could help to identify local differences in deformation and damage-relevant stress states. Furthermore, the influence of different mesh types on the calculated stress states requires additional investigation to determine whether observed differences in plastic deformation originate from numerical effects or from actual variations in deformation induced by different pass schedules, even if the total degree of deformation remains constant. In addition, the measured stress states provide an opportunity to experimentally reproduce the flat rolling process using scaled model experiments, which would allow for a faster and more efficient evaluation of different processing strategies. Prior to such investigations, experimental validation and a comparison of damage evolution between the rolling process and the model experiments will be necessary. A key challenge in this context will be the identification of suitable loading conditions. In accordance with the framework proposed by Bai Wierzbicki [3], loading paths between uniaxial tension, compression, and torsion represent an obvious choice. However, for stress states characterized by negative stress triaxiality combined with a positive Lode angle parameter, the realization of appropriate loading conditions may be challenging. A detailed discussion of these scenarios, however, goes beyond the scope of this work.

Summary

In this study, the influence of different cold rolling pass schedules on the mechanical response, microstructure, and stress state evolution of a micro-alloyed S355 steel was investigated. The material serves as a base for DP800 steel production and was subjected to identical total thickness reductions

but varying numbers of rolling passes. Experimental rolling tests and mechanical characterization were combined with finite element simulations to establish links between processing conditions, resulting microstructural features, and deformation-induced stress states. Tensile testing revealed that variations in pass schedules lead to measurable, albeit subtle, differences in yield strength, fracture strain and work hardening behavior, despite identical overall deformation and the absence of intermediate heat treatments. Microstructural analysis using EBSD and light optical microscopy revealed the expected pronounced grain elongation aligned with the rolling direction. While ferrite grains can still be reasonably approximated by elongated ellipses, the pearlite phase is characterized by very high aspect ratios and a pronounced banded morphology, which challenges the common assumption of ellipsoidal grain representations. Finite element simulations of the flat rolling process provided detailed insight into the evolution of stress triaxiality and Lode angle parameter throughout deformation. Although the overall stress-state trajectories were similar for all pass schedules, increasing the number of passes led to a smoother stress evolution with reduced stress peaks at pass entry and exit. This stabilization of the stress state suggests a potential reduction in damage initiation during rolling, offering a possible explanation for the enhanced damage tolerance reported for multi-pass rolling in dual-phase steels. Overall, the results demonstrate that the number of rolling passes, even at constant total reduction, influences both microstructural morphology and local stress states in a non-trivial manner. The combined experimental-numerical methodology provides a robust framework for future investigations, particularly for the development of representative volume elements and material models that account for deformation-induced microstructures prior to intercritical annealing.

Acknowledgement

This research was funded by Deutsche Forschungsgemeinschaft (DFG, German Research Foundation; Projectnumber 278868966 – TRR 188; Damage Controlled Forming Processes, subproject A08).

References

[1] FEHLEMANN, Niklas. (2025). Process – structure – property relations in DP800 investigated using representative volume elements. 995-1004. 10.21741/9781644903599-107.

[2] FEHLEMANN, N. et al. Investigation of Damage-Controlling Process-Parameters During Cold Rolling on the Impact Toughness of DP800 Steel Under Crash Loading Stress States. Proceedings of the 14th International Conference on the Technology of Plasticity - Current Trends in the Technology of Plasticity. Cham: Springer Nature Switzerland, 2024.

[3] BAI, Y., T. WIERZBICKI. A new model of metal plasticity and fracture with pressure and Lode dependence. International Journal of Plasticity. 2008-06, 24, pp. 1071–1096. Available from DOI: 10.1016/j.ijplas.2007.09.004.

[4] GAO, X.; G. ZHANG, C. ROE. A Study on the Effect of the Stress State on Ductile Fracture. International Journal of Damage Mechanics. 2010, 19(1), pp. 75–94. Available from DOI: 10.1177/1056789509101917.

[5] Sai Rajeshwari Kondavalasa, Aditya Prakash, Rohit Jagtap, Sankaran Shanmugam, I. Samajdar, Vijay K. Vasudevan, Gerhard Wilde, On the comparison of graded microstructures developed through High Reduction (per pass) Cold Rolling (HRCR) and Ultrasonic Nanocrystal Surface Modification (UNSM) in nickel-base Alloy 602CA, Materials Characterization, Volume 153, 2019, Pages 328-338, ISSN 1044-5803, DOI: 10.1016/j.matchar.2019.05.021.

[6] JIN, S.; H. ZEDONG, L. YUAN. Software implementation of corn grain morphology detection based on OpenCV. In: 2017 13th IEEE International Conference on Electronic Measurement and Instruments (ICEMI). 2017, pp. 412–415. Available from DOI: 10.1109/ICEMI.2017.8265837.

[7] Wang, Shuhan & Dunlap, Anthony & Möhring, Kerstin & Lohmar, Johannes & Schwedt, Alexander & Aretz, A. & Walther, Frank & Hirt, Gerhard. (2020). Torsion plastometer trials to investigate the effect of non-proportional loading paths in caliber rolling on damage and performance of metal parts. Production Engineering. 14. 10.1007/s11740-019-00949-5.

[8] Mahmoudi, Kasra & Haji Aboutalebi, Farhad & Sadeghi Nezhad, Soheil. (2025). Proposing a new 2D Bai-Wierzbicki (BW) ductile damage model for sheet metal forming processes. The International Journal of Advanced Manufacturing Technology. 1-15. 10.1007/s00170-025-17042-0.

[9] Kevarajan, Karthiga & Marimuthu, Prakash & Ramesh, A.. (2012). FEM analysis of effect of rolling parameters on cold rolling process. Bonfring Int J Ind Eng Manag Sci. 2. 35-40.

[10] Graça, Ana & Vincze, Gabriela. (2021). A Short Review on the Finite Element Method for Asymmetric Rolling Processes. Metals. 11. 762. 10.3390/met11050762.

[11] Tonini Button, S. (2013). Tribology in metal forming processes. In J. P. Davim (Ed.), Tribology in manufacturing technology (pp. 103–120). Springer Berlin Heidelberg. DOI: 10.1007/978-3-642-31683-8_3.

[12] Wei, Zhang & Wen, Jian-Feng & Zhang, Xian-Cheng & Tu, Shan-Tung. (2019). Effects of the stress state on plastic deformation and ductile failure: Experiment and numerical simulation using a newly designed tension-shear specimen. Fatigue & Fracture of Engineering Materials & Structures. 42. 2079-2092. 10.1111/ffe.13084.

[13] Flanagan, Francis & O'Connor, Alison & Erfanian, Mozhdeh & Music, Omer & Brambley, Edward & O'Kiely, Doireann. (2024). Careful finite element simulations of cold rolling with accurate through-thickness resolution and prediction of residual stress. 10.48550/arXiv.2408.03242.

[14] Bessa, M. & Elkhodary, K. & Liu, Wing & Belytschko, Ted & Moran, Brian. (2013). Nonlinear Finite Elements for Continua and Structures, Second Edition. Solution Manual. DOI: 10.13140/RG.2.1.2800.0089.

[15] Zienkiewicz OC, Taylor RL, Zhu JZ. The finite element method: Its basis and fundamentals. 7th ed. Oxford: Butterworth-Heinemann; 2013.

[16] Roters, F., Eisenlohr, P., Bieler, T. R., & Raabe, D. (2010). Crystal plasticity finite element methods: Fundamentals and applications. Acta Materialia, 58(4), 1152–1211. DOI: 10.1016/j.actamat.2009.10.058.

[17] M. Henrich, N. Fehlemann, F. Bexter, M. Neite, L. Kong, F. Shen, M. Könemann, M. Dölz, and S. Münstermann, DRAGen - A deep learning supported RVE generator framework for complex microstructure models. Heliyon, 8 (2023) e19003. DOI: 10.1016/j.heliyon. 2023.e19003.

[18] Seibert, Paul & Raßloff, Alexander & Kalina, Karl Alexander & Ambati, Marreddy & Kästner, Markus. (2022). Microstructure Characterization and Reconstruction in Python: MCRpy. Integrating Materials and Manufacturing Innovation. 11. 1-17. DOI: 10.1007/s40192-022-00273-4.

The publication of this article was funded by the RWTH Aachen University 10.13039/501100007210